ANTIOXIDANTS & REDOX SIGNALING
Volume 13, Number 9, 2010

DOI: 10.1089/ars.2010.3099

FORUM REVIEW ARTICLE

Structural Basis for the Disulfide Relay System in the Mitochondrial Intermembrane Space

Toshiya Endo, Koji Yamano, and Shin Kawano

Abstract

Mitochondria contain two biological membranes. Although reducing agents can diffuse from the cytosol into the intermembrane space (IMS) between the outer and inner mitochondrial membranes, the IMS has a dedicated disulfide relay system to introduce disulfide bonds into mainly small and soluble proteins. This system consists of two essential proteins, a disulfide carrier Tim40/Mia40 and a flavin-dependent sulfhydryl oxidase Erv1, high-resolution structures that have recently become available. Tim40/Mia40 transfers disulfide bonds to newly imported IMS proteins by dithiol/disulfide exchange reactions involving mixed disulfide intermediates. Tight folding by introduction of disulfide bonds prevents egress of these small IMS proteins, resulting in their selective retention in the compartment. After disulfide transfer from Tim40/Mia40 to substrate proteins, Tim40/Mia40 is reoxidized again by Erv1, which is then oxidized by electron transfer to either cytochrome *c* or molecular oxygen. Here we review the recent advancement of the knowledge on the mechanism of the disulfide relay system in the mitochondrial IMS, especially shedding light on the structural aspects of its components. *Antioxid. Redox Signal.* 13, 1359–1373.

Tim40/Mi40-Erv1 System in the Mitochondrial Intermembrane Space

EUKARYOTIC CELLS ARE DIVIDED into many membrane-bounded organelles that perform distinct cellular functions. Until several years ago, the endoplasmic reticulum (ER) was believed to be the only cellular compartment in which proteins fold oxidatively (*i.e.*, with the acquisition of disulfide bonds). However, in 2004 two groups independently identified the new yeast component Tim40 (*T*ranslocase of *I*nner mitochondrial *M*embrane)/Mia40 (*M*itochondrial *I*ntermembrane space import and *A*ssembly), a protein that mediates protein transport into the aqueous compartment between the mitochondrial outer and inner membranes, known as the mitochondrial intermembrane space (IMS) (17, 62, 73). Tim40/Mia40 was subsequently shown by Mesecke *et al.* (56) to function as a disulfide carrier to introduce disulfide bonds into proteins that are synthesized in the cytosol and subsequently imported into the mitochondrial IMS (Fig. 1). The mitochondrial IMS is thus the second eukaryotic cellular component found to promote disulfide bond formation in proteins (for reviews, see 24, 34, 35, 47, 72).

Suggested substrate proteins for Tim40/Mia40 are IMS proteins of, in most cases, less than 20 kDa containing cysteine motifs such as twin CX_3C and twin CX_9C, the latter being the same motif as found in Tim40/Mia40 itself (Table 1). For example, small Tim proteins from yeast (Tim8, Tim9, Tim10, Tim12, and Tim13), which function as chaperones to facilitate the transport of hydrophobic proteins through the aqueous IMS, contain the twin CX_3C motif. The sequence around the CX_3C motifs may well be recognized by Tim40/Mia40 (58), and indeed such a potential signature sequence was identified for Tim9 recently (59). The signature sequence is characterized by the essential Leu at four-residue upstream of the CX_3C motif. Recent genome-wide analyses of yeast *Saccharomyces cerevisiae* showed that, in addition to Tim40/Mia40 (40 kDa), ~14 different mitochondrial proteins with a size of 9–18 kDa possess the twin CX_9C motif (53) (Table 1). Those small CX_9C proteins include Cox17, which is a copper-binding protein and mediates copper transfer to cytochrome *c* oxidase (14, 53), and Cox19, which is also a copper-binding protein and presumably performs similar functions to Cox17 (68). Although a signature sequence for the CX_9C motif to be recognized by Tim40/Mia40 has not yet been identified, sequence comparison of those CX_9C containing proteins revealed the conserved hydrophobic residues between the cysteine residues in their CX_9C motif ($CX_6\Phi\chi\chi C$), which resembles the signature sequence for the CX_3C motif (53).

High-resolution structures have been determined for several IMS proteins containing the twin CX_3C or twin CX_9C motifs: Tim9 and Tim10 from yeast (5) and human (78), Tim8

Department of Chemistry, Graduate School of Science, Nagoya University, Nagoya, Japan.

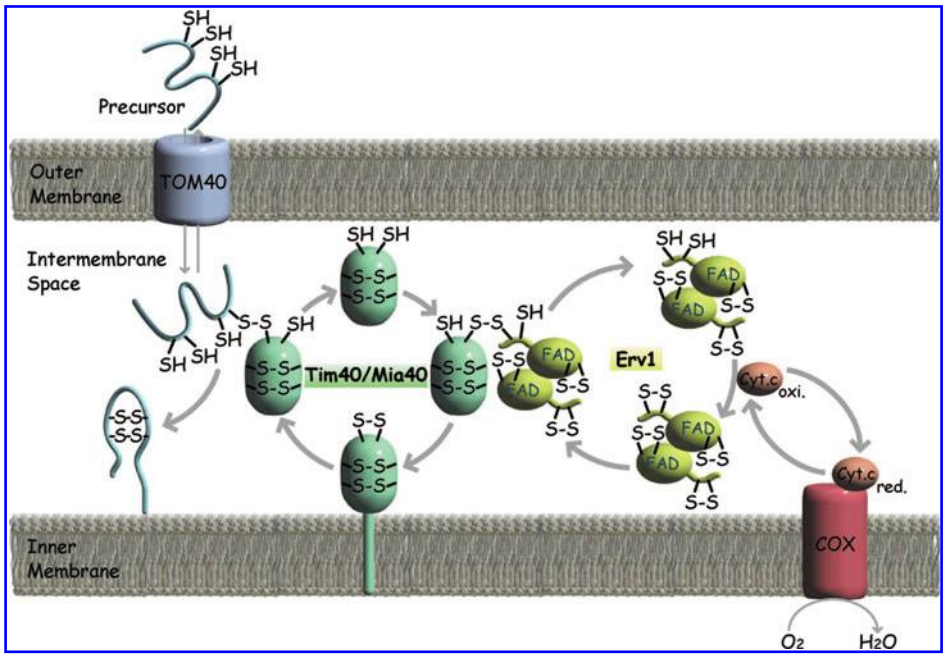

FIG. 1. Tim40/Mia40 disulfide relay system in the mitochondrial IMS. The disulfide relay system consisting of Tim40/Mia40 and Erv1, and its disulfide-transfer or electron transfer reactions are schematically shown. Cyt c, cytochrome *c*; COX, cytochrome oxidase; precursor, substrates for Tim40/Mia40; TOM40, the TOM40 complex; (For interpretation of the references to color in this figure legend, the reader is referred to the web version of this article at www.liebertonline.com/ars).

Table 1. IMS Proteins with Disulfide Bonds (Possible Substrates for Tim40/Mia40)

Protein	*Size (kDa)*[1]	*Motif*	*Function*	*Reference*[2]	*Reference*[3]	*Reference*[4]
Rip1/Rieske FeS	23	other	Cytochrome bc_1 complex function	41		
Qcr6	17	other	Cytochrome bc_1 complex function	41		
Sod1	16	other	Superoxide dismutase	49	66	29
Ccs1	27	other	Sod1 assembly	49	66	29
Sco1	33	CX_3C	Cytochrome oxidase assembly			6
Sco2	35	CX_3C	Cytochrome oxidase assembly			8
Cox11	34	CX_3C	Cytochrome oxidase assembly			7
Cox12	10	twin CX_9C	Cytochrome oxidase assembly	76		48
Cox17	8	twin CX_9C	Cytochrome oxidase assembly	1, 4	17, 73	
Cox19	11	twin CX_9C	Cytochrome oxidase assembly		17	64
Cox23	17	twin CX_9C	Cytochrome oxidase assembly			11
Pet191	12	twin CX_9C	Cytochrome oxidase assembly			45
Cmc1	13	twin CX_9C	Cytochrome oxidase assembly		53	38
Cmc2	13	twin CX_9C	Cytochrome oxidase assembly		53	
Coa4/Cmc3	17	twin CX_9C	Cytochrome oxidase assembly		53	
Cmc4	8	twin CX_9C	Unknown function		53	
Mrp10	11	twin CX_9C	Mitochondrial ribosomal protein			43
Emi1	21	twin CX_9C	Mitochondrial morphology			53
Som1	8	twin CX_9C	Inner membrane peptidase subunit			53, 42
Mic14	14	twin CX_9C	Unknown function		30	
Mic17	17	twin CX_9C	Unknown function		30	
Mdm35	10	twin CX_9C	Mitochondrial morphology		30	
Tim8	10	twin CX_3C	Protein import	21	17	
Tim9	10	twin CX_3C	Protein import	20	17, 62	
Tim10	10	twin CX_3C	Protein import	20	17, 73	
Tim12	12	twin CX_3C	Protein import	12	31	
Tim13	11	twin CX_3C	Protein import	21	17, 62, 73	
Tim40/Mia40	45	twin CX_9C	Protein import, oxidative folding	75	18	
Erv1	22	other	Oxidative folding, FeS cluster export	13	30, 74	50

[1]Molecular mass of precursor proteins.
[2]Reference that experimentally confirmed the presence of disulfide bond(s).
[3]Reference that experimentally confirmed that the protein was a substrate for Tim40/Mia40.
[4]Others.

and Tim13 from yeast (15), Cox17 from yeast (1) and human (4, 9), and Tim40/Mia40 from yeast (44) and human (10). The structures show that the twin CX_3C or twin CX_9C motifs form similar helix-turn-helix folds, in which two helices in antiparallel orientation are connected by the two disulfide bonds (Fig. 2). Those closely related folds for the twin CX_3C and twin CX_9C motifs are at least partly stabilized by the presence of more apolar residues on the helix–helix interface of the two antiparallel helices (53) (Fig. 2).

Processes of import and subsequent disulfide transfer of mitochondrial proteins can be analyzed *in vitro* by incubation of radiolabeled substrate proteins with isolated mitochondria followed by SDS-PAGE or blue-native-PAGE under reducing and nonreducing conditions. Those *in vitro* import assays showed that substrate proteins for Tim40/Mia40, such as small Tim proteins, Cox17, and Cox19 form transient intermediates with Tim40/Mia40 via an intermolecular (mixed) disulfide bond immediately after crossing the outer membrane through the import channel of the TOM40 complex, a protein translocator in the outer membrane, to reach the IMS (Fig. 1) (17, 56, 62, 73). The substrate protein is subsequently released from Tim40/Mia40 to proceed to further assembly processes such as formation of the Tim9–Tim10 complex and TIM22 complex in the case of Tim9 and Tim10. Release of the substrate protein from Tim40/Mia40 appears rather slow as compared with formation of the mixed-disulfide intermediate, so that the intermediate comprised of Tim40/Mia40 and the substrate protein is transiently accumulated at least in *in vitro* import assays (17, 56, 62). Upon release of the substrate protein from Tim40/Mia40, a disulfide bond is transferred from Tim40/Mia40 to the substrate protein via the intermolecular disulfide bond, leaving Tim40/Mia40 in the reduced state (56). Reduced Tim40/Mia40 requires reoxidation to become active as a disulfide carrier to introduce disulfide bonds into substrate proteins in the next round of disulfide bond transfer. This reoxidation of Tim40/Mia40 is achieved by Erv1, an essential sulfhydryl oxidase in the mitochondrial IMS (Fig. 1) (56).

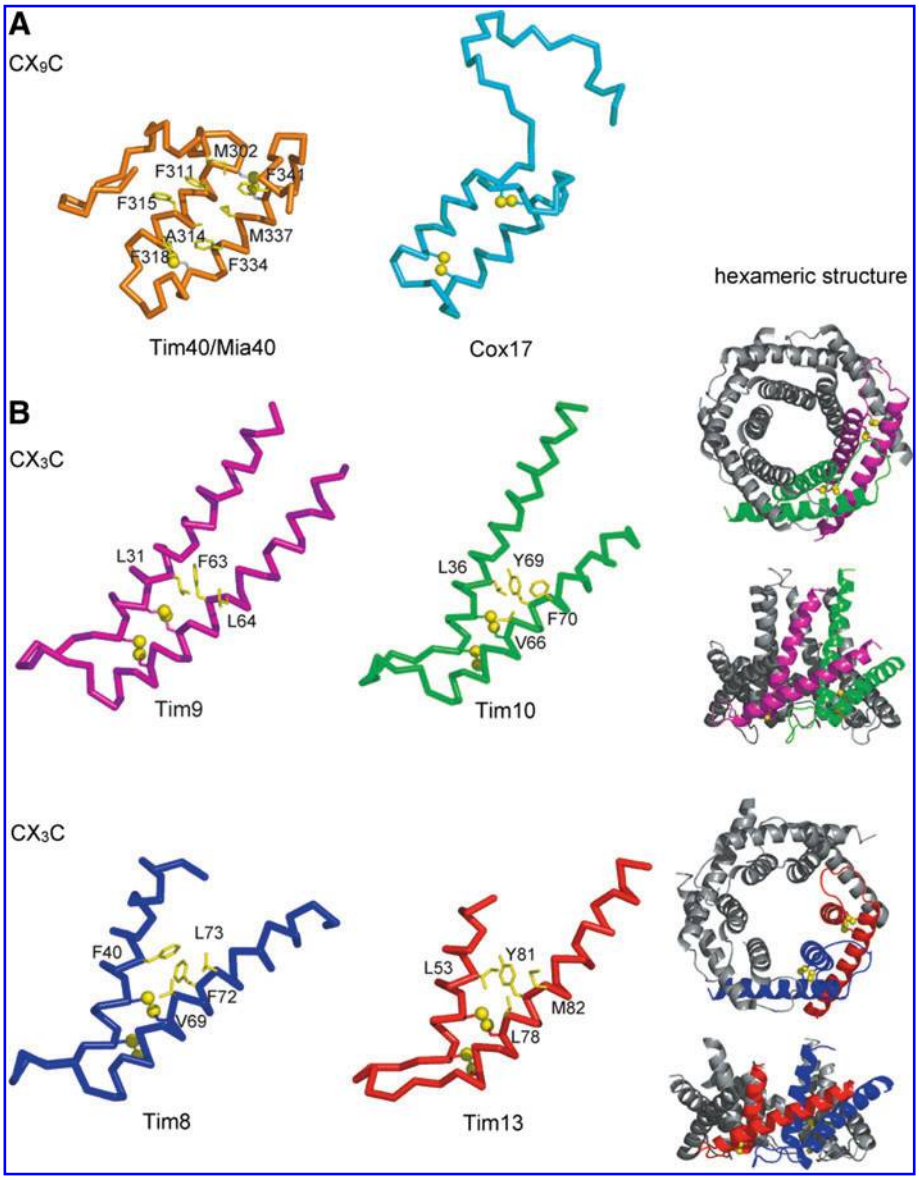

FIG. 2. Comparison of the tertiary structures of the CX_9C motifs (A) and CX_3C motifs (B) in various IMS proteins. The sulfur atoms of the two disulfide bonds are presented as *yellow spheres*. Side chains of the hydrophobic residues stabilizing the anti-parallel α-helical hairpins are shown in *yellow stick form*. Side views and aerial views of the structures of the Tim9–Tim10 and Tim8–Tim13 hexameric complexes are shown as *ribbon diagrams* on the right (Tim9 is in *magenta*, Tim10 in *green*, Tim8 in *dark blue*, and Tim13 in *red*). PDB-ID for each structure is yeast Tim40/Mia40 (2ZXT), yeast Cox17 (1U96), yeast Tim9 (3DXR), yeast Tim10 (3DXR), yeast Tim8 (3CJH), and yeast Tim13 (3CJH). (For interpretation of the references to color in this figure legend, the reader is referred to the web version of this article at www.liebertonline.com/ars).

Tim40/Mia40 as a Disulfide Carrier

Tim40/Mia40 is an oxidized disulfide carrier in the mitochondrial IMS and is conserved in most eukaryotic cells. Tim40/Mia40 contains a conserved C-terminal core domain of about 60 amino-acid residues whereas its N-terminal region is variable in length and sequence (Fig. 3). Tim40/Mia40 in fungi has a long N-terminal region and is anchored to the inner membrane by the N-terminal transmembrane (TM) segment, exposing the C-terminal region to the IMS (62, 73). On the other hand, Tim40/Mia40 in animals and plants has only a short N-terminal region lacking the TM segment and is soluble in the IMS (37). The N-terminal anchor of fungal Tim40/Mia40 to the inner membrane is not essential for its functions, and for example, soluble human MIA40 is fully functional in yeast cells (37, 62, 73).

The C-terminal core domain of Tim40/Mia40 bears six conserved cysteine residues (residues 296, 298, 307, 317, 330, and 340 in yeast; hereafter termed C1–C6 from the N-terminus to the C-terminus), which form an invariant CPC motif (C1 and C2), followed by a twin CX_9C motif (C3, C4, C5, and C6). Under physiological conditions, Tim40/Mia40 is mainly in a fully oxidized state containing the three disulfide pairs, C1–C2, C3–C6, and C4–C5 (33, 56, 75). Among those three disulfide bonds, the C1–C2 pair is susceptible to reduction, and can be partly reduced both *in vitro* and *in vivo* (33). Amino acid replacement of the conserved cysteine residues of yeast Tim40/Mia40 with serine revealed that the C2S mutation was lethal and impaired the interaction of Tim40/Mia40 with its specific oxidase Erv1 (described later) (44, 75). The yeast strains with the C1S mutation or C1,2S mutation were also lethal (44) or exhibited severe growth defects (75). When small Tim proteins were incubated *in vitro* with isolated mitochondria with the C1,2S mutation, a mixed-disulfide intermediate with mutant Tim40/Mia40 did not accumulate (75). These observations suggest that the redox-sensitive first C1–C2 disulfide bond or CPC motif mediates disulfide transfer to substrate proteins. On the other hand, the C3,6S or C4,5S mutation did not affect the overall structures of Tim40/Mia40 (Fig. 4, left panel) (44), yet they destabilized the Tim40/Mia40 structure since the C3,6S and C4,5S Tim40/Mia40 mutants were readily unfolded in the presence of 6 *M* urea as monitored by circular dichroism (CD) measurements, whereas wild-type Tim40/Mia40 and the C1,2S Tim40/Mia40 mutant resisted unfolding (Fig. 4, right panel) (44).

Tertiary Structure of Tim40/Mia40

High-resolution structures were recently determined for human MIA40 by NMR (10) and yeast Tim40/Mia40 by X-ray diffraction analyses (44). Banci *et al.* analyzed the NMR spectra of 142-residue human MIA40 and found that regions 1–41 and 107–142 are highly flexible and do not exhibit any secondary structures (10). They thus determined the solution NMR structure of the folded core domain (residues 41–105 corresponding to residues 284–348 of yeast Tim40/Mia40; Fig. 5A) of human MIA40, in which the disulfide bond C1–C2 is reduced by a low concentration of dithiothreitol (DTT) while the other two disulfide bonds remain oxidized (Fig. 5B).

The X-ray crystal structure was independently determined for the core IMS domain of yeast Tim40/Mia40 (44). Since the N-terminal TM segment of yeast Tim40/Mia40 is not essential for its function (62), the recombinant version of the residues 284–365 (Tim40/Mia40C4), which includes a minimal functional unit of residues 284–352 in the IMS domain (33), was chosen for the structural analyses. A large soluble protein, maltose binding protein (MBP), was attached at the N-

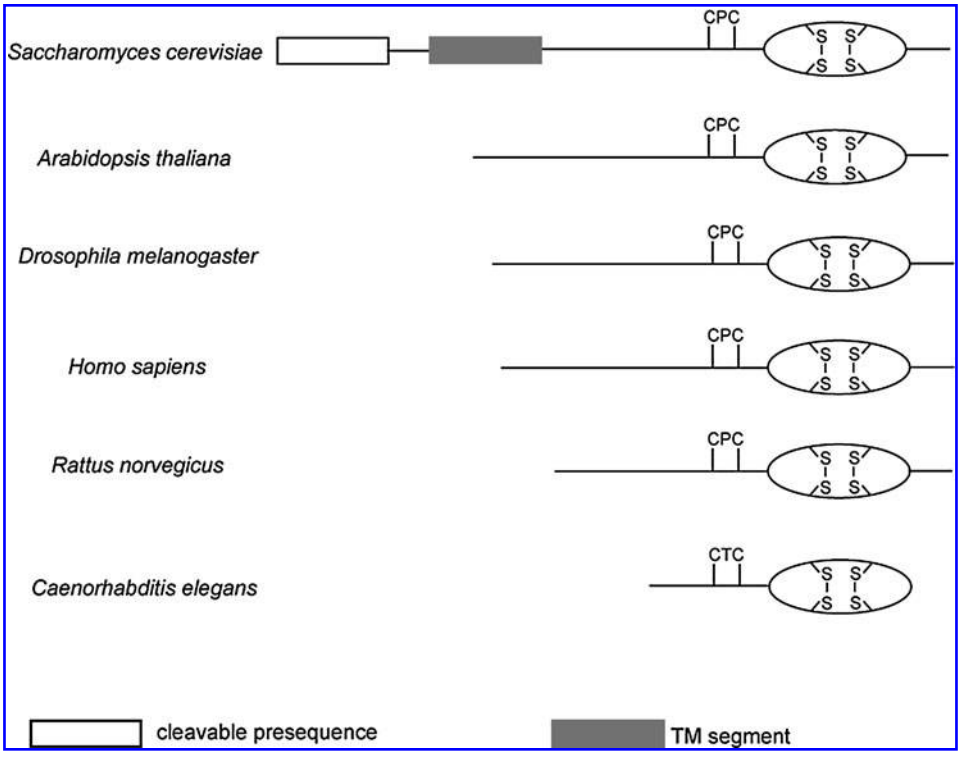

FIG. 3. Schematic diagrams of Tim40/Mia40 from various organisms. A cleavable presequence, a TM segment, conserved CPC (C1–C2), C3–C6, and C4–C5 disulfide bonds are indicated.

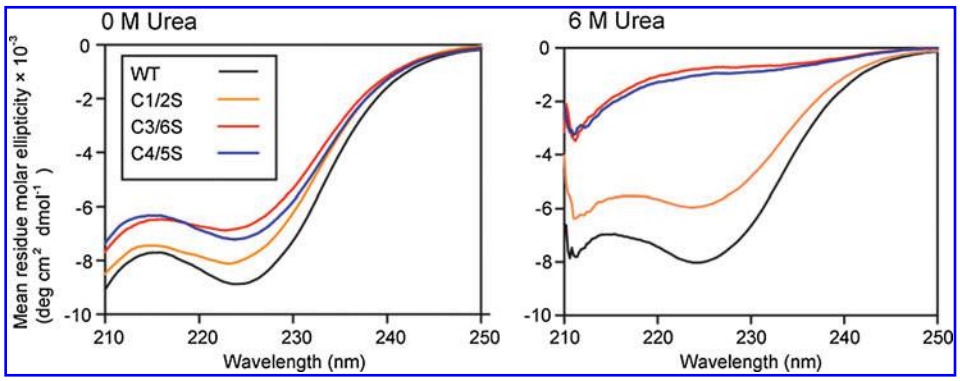

FIG. 4. CD spectra of the Cys-to-Ser mutants of the yeast Tim40/Mia40C4 domain. CD spectra of wild-type (WT) Tim40/Mia40C4 (plus four residues, *i.e.,* residues 280–365) and its Cys-to-Ser mutants in the absence (*left*) and presence (*right*) of 6 *M* urea. (We recently found that the CD spectra (Fig. S3) in Kawano S, Watanabe N, and Endo T, unpublished results, were presented as raw data, but not as those in mean residue molar ellipticity. Therefore the CD spectra in this figure are correctly presented spectra in mean residue molar ellipticity.) In the presence of 6 *M* urea (*right panel*), while the CD spectra of WT and C1/2S mutant Tim40/Mia40C4 resemble those in the absence of urea (*left panel*) and still exhibit negative bands around 220–225 nm, which are typical for the presence of α-helices, C3/6S and C4/5S mutants lack those negative bands, suggesting their denaturation by urea. Far-UV CD spectra of 10 μ*M* WT and mutant Tim40/Mia40C4 were recorded in 20 m*M* Tris-HCl, pH 7.5, 50 m*M* NaCl at 25°C on a JASCO J-720 spectropolarimeter. (For interpretation of the references to color in this figure legend, the reader is referred to the web version of this article at www.liebertonline.com/ars).

terminus of Tim40/Mia40C4 via a 16-residue spacer segment at the DNA level to further increase solubility of the core domain. The resultant fusion protein (MBP–Tim40/Mia40C4) with three disulfide bonds was successfully crystallized, and the crystal structure of MBP–Tim40/Mia40C4 was determined at a resolution of 3.0Å using coordinates of MBP as a search model (Fig. 5B).

The NMR structure of the human MIA40 core domain and X-ray structure of yeast Tim40/Mia40C4 resemble each other quite well, with a root mean square deviation for C_α positions of 1.9 Å (Fig. 5D), irrespective of the difference in the oxidation state of the CPC motifs between the two structures. The determined Tim40/Mia40 core structures consist of a long N-terminal loop followed by two 13-residue α-helices H1 and H2 (Figs. 5B and 5C). Helices H1 and H2 form an antiparallel α-helical hairpin, in which H1 and H2 are connected by the two disulfide bonds C3–C6 (Cys307–Cys340 in yeast Tim40/Mia40 and Cys64–Cys97 in human MIA40) and C4–C5 (Cys317–Cys330 in yeast Tim40/Mia40 and Cys74–Cys87 in human MIA40). Clearly the two disulfide bonds stabilize the antiparallel hairpin of the H1 and H2 helices, while those two disulfide bonds are not essential for formation of the hairpin structure as described above (Fig. 4).

The N-terminal loops containing the first C1–C2 disulfide bond or CPC motif (Cys296–Cys298 in yeast Tim40/Mia40 and Cys53–Cys55 in human MIA40) of the two structures match each other, suggesting that the N-terminal loop is structurally rigid or precisely positioned within each protein domain. The rigid conformations of the N-terminal loop in yeast and human MIA40 apparently rely on the interactions between the hydrophobic residues in the loop and those located on one side of the antiparallel α-helical hairpin (Figs. 6A and 6B). Those hydrophobic interactions position the C1-C2 disulfide bond in a solvent exposed conformation, which explains well its sensitivity to reduction by DTT.

Disulfide Bond Transfer by Tim40/Mia40

One of the notable features of the determined yeast and human MIA40 core domains is the presence of rather wide-open hydrophobic regions on their molecular surfaces. In the crystal structure of yeast Tim40/Mia40C4, the hydrophobic region (10Å×12Å) is formed by the hydrophobic side chains of the residues such as Phe311, Phe315, Phe318, Val319, Phe334, Met337, and Phe341, which protrude from helices H1 and H2, on the concave side of the fruitdish-like molecule (Fig. 6A; Fig. 7A, left panel). In contrast, the other side of the yeast Tim40/Mia40C4 molecule is prevailed by hydrophilic residues (Fig. 6B; Fig. 7A, right panel). In the solution NMR structure of the human MIA40 core domain, presence of a similar hydrophobic region on one side of the molecule is obvious as well (Fig. 6B, left panel). Interestingly, in the crystal structure of MBP–Tim40/Mia40C4, an 11-residue segment of the linker between MBP and Tim40/Mia40C4 is accommodated, partly forming a helical structure, in the hydrophobic concave region. The linker segment may well mimic a substrate peptide segment recognized by Tim40/Mia40C4. The residues in contact with the 11-residue linker segment are shown in magenta on the yeast Tim40/Mia40C4 structure (Fig. 8A), and corresponding residues for the human MIA40 core domain are in orange (Fig. 8B).

The roles of this hydrophobic putative substrate-binding region in Tim40/Mia40 functions were tested by amino acid replacement of one of the four hydrophobic phenylalanine residues (Phe311, Phe315, Phe318, or Phe334) that are in contact with the linker segment (44). When Phe311, Phe315, Phe318, or Phe334 of Tim40/Mia40 was replaced with a hydrophilic glutamate residue, F315E and F318E mutations were lethal while F311E and F334E mutations led to temperature-sensitive lethality at 37°C, whereas replacement of those residues with hydrophobic alanine or leucine did not cause growth defects. Indeed, NMR titration analyses showed that the F318E mutation lowered the affinity of the Tim40/Mia40 core domain for the signature peptide derived from the authentic substrate Tim9 (59) from K_d of ~ 0.7 m*M* to K_d of ~3.6 m*M* (44).

In vitro import analyses showed that the F334E mutation retarded formation of the Tim9–Tim40/Mia40 intermediate complex and mature TIM22 complex probably due to the reduced level of Erv1, although the reason for the reduction of the Erv1 level was unclear (44). On the other hand, F311E

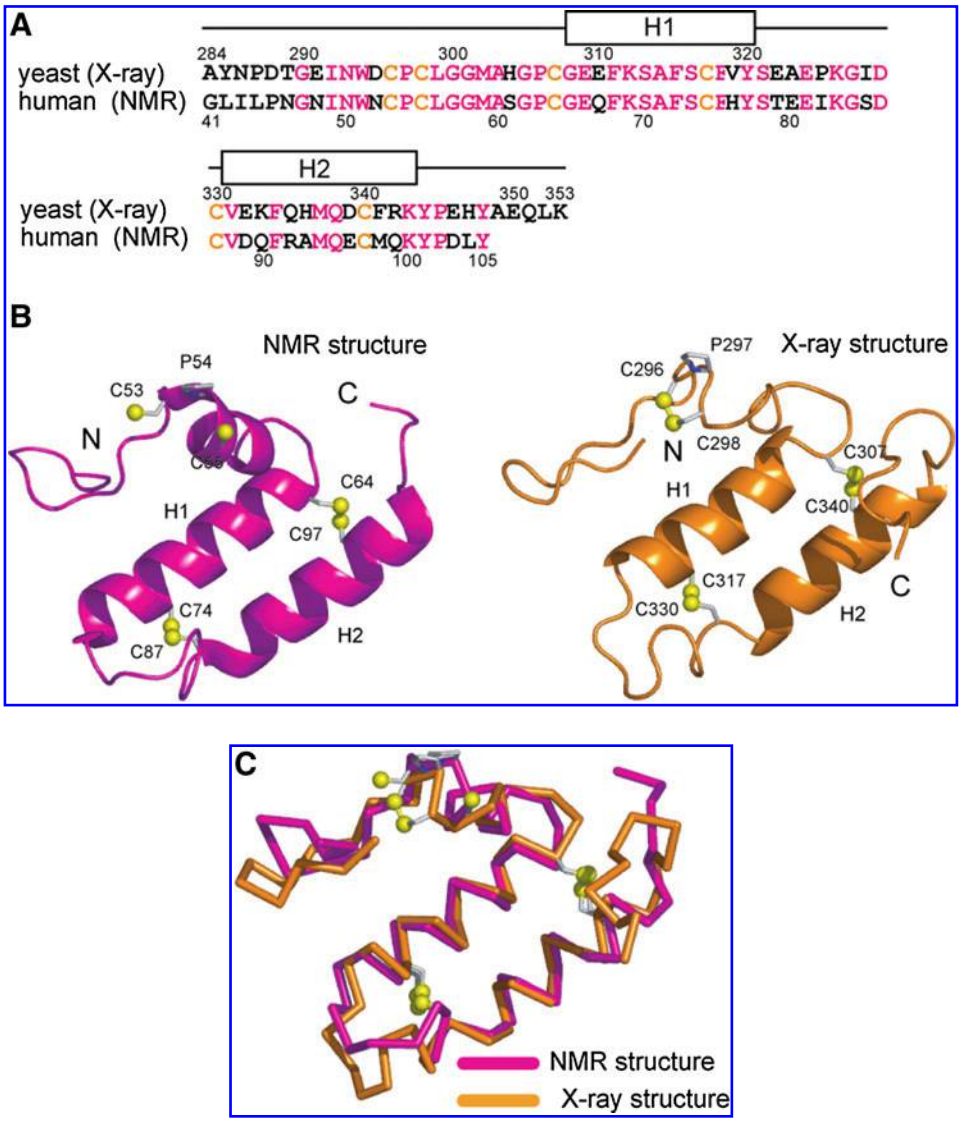

FIG. 5. Solution NMR and X-ray crystal structures of the Tim40/Mia40 core domains. (**A**) Amino-acid sequences of the domains of yeast Tim40/Mia40C4 and human MIA40 core domain whose structures were determined by X-ray crystallography and NMR, respectively. Identical amino acid residues are shown in *magenta*, and conserved Cys in *orange*. Two 13-residue α-helices H1 and H2 are indicated above the sequences. (**B**) The NMR structure of the human MIA40 core domain (2K3J) and the X-ray crystal structure of yeast Tim40/Mia40C4 (2ZXT) are shown in *magenta* and *orange ribbon model*, respectively. The sulfur atoms of the three disulfide bonds are presented as *yellow spheres*. (**C**) Superimposition of the solution NMR structure of the human MIA40 core domain (*magenta*) and the X-ray crystal structure of yeast Tim40/Mia40C4 (*orange*) in stick form. The S atoms are shown as in (**B**). (For interpretation of the references to color in this figure legend, the reader is referred to the web version of this article at www.liebertonline.com/ars).

mitochondria containing normal levels of Erv1 and other translocator components allowed imported Tim9 to form the Tim9–Tim40/Mia40 intermediate normally, but its dissociation from Tim40/Mia40 and subsequent formation of the final TIM22 complex was significantly retarded (44).

Interestingly, temperature-sensitive growth defects of substrate-binding region mutants (F311E and F334E) were suppressed by overexpression of Erv1 from the multi-copy plasmid (44). Consistently, overexpression of Erv1 in F311E mitochondria partly relieved the assembly defects of Tim9 *in vitro* (44). Although overexpression of Erv1 did not change the ratio of the oxidized and reduced forms of Tim40/Mia40, it significantly increased the amount of the Tim40/Mia40-Erv1 complex with an intermolecular disulfide bond (44). Therefore, Phe311 in the hydrophobic region of Tim40/Mia40 might not be important for mere substrate binding, but for the later step of disulfide bond transfer perhaps involving the substrate Tim40/Mia40-Erv1 ternary complex (71) as well.

Disulfide-Transfer Coupled Import by Tim40/Mia40

Although Tim40/Mia40 can introduce disulfide bonds into several larger proteins including Tim40/Mia40 (47, 67), most substrates for Tim40/Mia40 are less than 20 kDa (Table 1). Transfer of disulfide bonds into those small proteins by Tim40/Mia40 may well couple with their vectorial translocation across the outer membrane. What is the role of Tim40/Mia40 in such coupled import of small IMS proteins?

The mitochondrial outer membrane contains a translocator, the TOM40 complex, which functions as a general entry gate for most mitochondrial precursor proteins (19, 25, 63). The TOM40 complex consists of the import channel mainly composed of Tom40 and receptor subunits such as Tom20, Tom22, and Tom70. Small Tim proteins such as Tim13 appear to utilize the Tom40 channel since their *in vitro* import is competitively inhibited by a large amount of matrix-targeted precursor proteins (55). However on the other hand, specific removal of the receptor subunit Tom20 or Tom22, or even trypsin treatment of mitochondria to remove any surface exposed receptor domains did not affect the *in vitro* import of small Tim proteins (55, 80). The outer mitochondrial membrane does not have any transmembrane proton or ion gradient and the IMS lacks any ATP-dependent chaperones that function as an import motor. Indeed, *in vitro* import of small Tim proteins does not depend on ATP or membrane potential

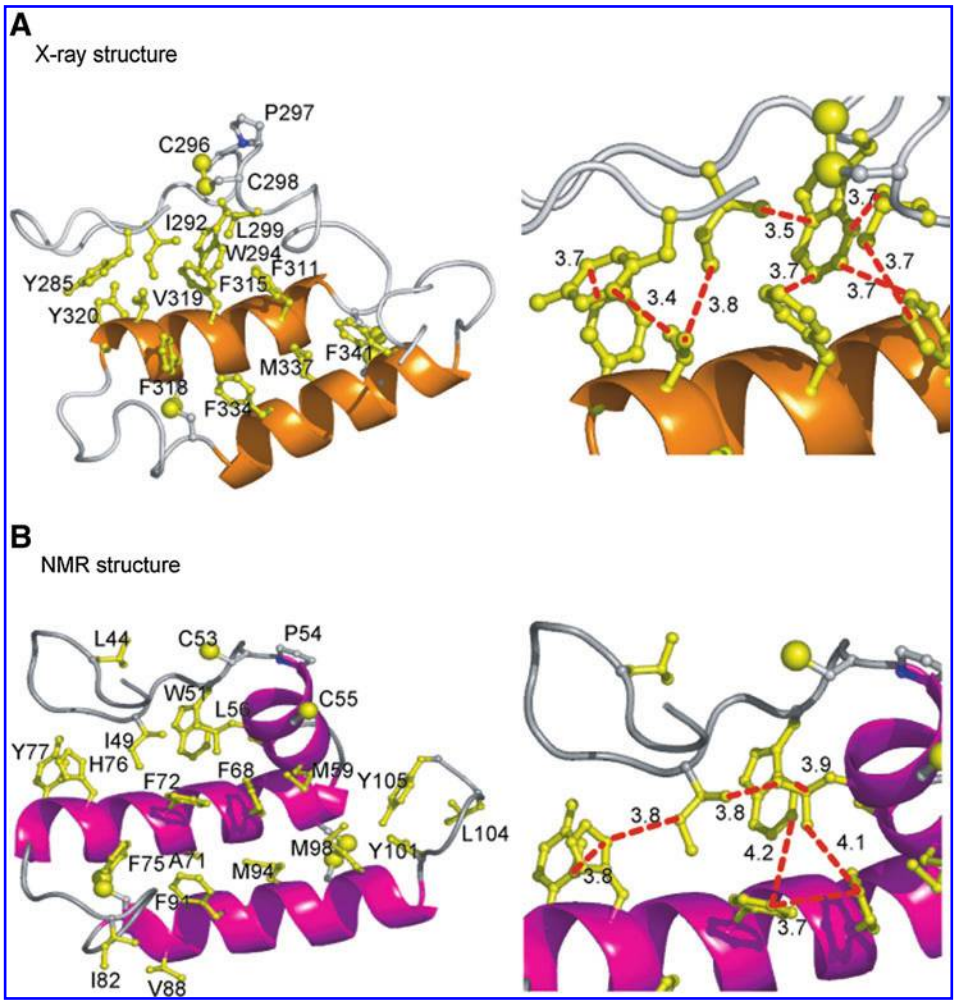

FIG. 6. Hydrophobic residues in the N-terminal loop and the antiparallel α-helical hairpin of yeast Tim40/Mia40C4 and the human MIA40 core domain. The X-ray crystal structure of yeast Tim40/Mia40C4 (**A**) and the NMR structure of the human MIA40 core domain (**B**) are shown in *magenta* and *orange ribbon model*, respectively. The sulfur atoms are shown as in Figure 5B. Side chains of the hydrophobic residues in the N-terminal loop and the antiparallel α-helical hairpin are shown in *yellow stick form* (*left panels*). Distances (Å) for the side chains of the hydrophobic residues (in the N-terminal loop and the first α-helix) in close proximity are indicated (*right panels*). (For interpretation of the references to color in this figure legend, the reader is referred to the web version of this article at www.liebertonline.com/ars).

across the inner membrane ($\Delta\psi$), which is essential for matrix-destined precursor proteins to cross the inner membrane (55). Therefore, active or vectorial passage of mitochondrial precursor proteins from the cytosol to the IMS through the TOM40 channel requires an ATP or $\Delta\psi$ independent mechanism to drive the import.

Generally, trapping of substrate precursor proteins on the *trans* side of the membrane could contribute to the unidirectionality of their import. Trapping can be achieved by cofactor binding, binding by chaperones, assembly with partner proteins, and spontaneous or facilitated folding of the proteins themselves. In the one extreme case of the fusion proteins with two domains with a spacer segment in between, they can form transient translocation intermediates that span the outer membrane with two domains exposed to the *cis* and *trans* sides of the outer membrane, and stability of the folded domains determine the directionality of the subsequent translocation (26). If the IMS domain is more stable than the cytosol domain, the outer membrane spanning intermediate will shift to the IMS whereas the more stable cytosol domain will shift it to the cytosol. When Tim8 was imported into isolated mitochondria *in vitro*, an oxidized monomer of Tim8 transiently accumulated after formation of the mixed-disulfide intermediate with Tim40/Mia40 but before assembly into the final Tim8–Tim13 complex (61). This oxidized monomeric Tim8 could be efficiently released to the supernatant after centrifugation of mitochondria only when the mitochondria were treated with DTT, suggesting that oxidized Tim8 was retained in the IMS while reduced Tim8 could diffuse back to the cytosol. Therefore, formation of the mixed-disulfide intermediates with Tim40/Mia40 and subsequent disulfide-assisted tight folding of the newly imported proteins in the IMS could serve as a mechanism to trap them on the *trans* (IMS) side of the membrane and prevent them from retrotranslocation to the cytosol.

In this connection, it is interesting to compare the import pathways for two classes of Tim40/Mia40 from different organisms. Fungal Tim40/Mia40 proteins including yeast Tim40/Mia40 are large (>25 kDa) and possess an N-terminal presequence while Tim40/Mia40 from higher eukaryotes usually retain the C-terminal core domain of fungal Tim40/Mia40 and do not posses a presequence (Fig. 3) (18). Yeast Tim40/Mia40 has an N-terminal presequence and is imported via the presequence-import pathway utilizing the TOM40 and TIM23 complexes in a $\Delta\psi$-dependent manner (18). The TM segment following the presequence arrests the translocation of Tim40/Mia40 in the inner membrane, so that the mature part is laterally released into the inner membrane with the topology that exposes the C-terminal domain to the IMS. Then Tim40/Mia40 introduces disulfide bonds into the newly

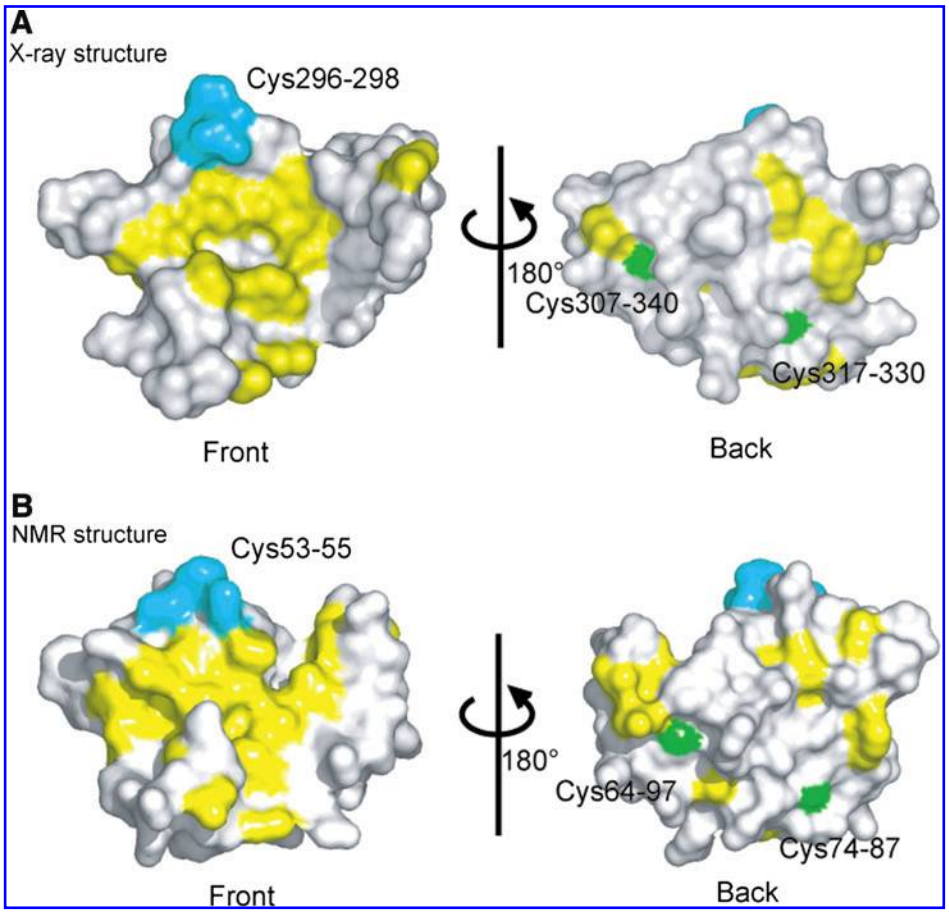

FIG. 7. Hydrophobic surface regions of yeast Tim40/Mia40C4 and the human MIA40 core domain. Side chains of hydrophobic residues (*yellow*), the CPC motif (*cyan*), and the C3–C6 and C4–C5 cysteine residues (*green*) are shown on the molecular surfaces of the X-ray crystal structure of yeast Tim40/Mia40C4 (**A**) and the NMR structure of the human MIA40 core domain (**B**). (For interpretation of the references to color in this figure legend, the reader is referred to the web version of this article at www.liebertonline.com/ars).

imported Tim40/Mia40 in the IMS. Therefore, import and disulfide transfer of yeast Tim40/Mia40 are carried out by different components and are therefore not coupled to each other. On the other hand, both human MIA40 and a truncated version or the core domain (residues 276–403) of yeast Tom40 were imported into mitochondria depending on the Tim40/Mia40-Erv1 system, but independently of $\Delta\psi$, like small IMS proteins (18). Therefore human MIA40 and even the core domain of yeast Tim40/Mia40 have sufficient mitochondrial targeting information and their import is accompanied with disulfide transfer from preexisting Tim40/Mia40. These results suggest that disulfide transfer by the Tim40/Mia40-Erv1 system in the IMS can drive protein translocation across the outer membrane if substrate proteins are small and represent one folding unit, thereby easily passing through the TOM40 channel by diffusion without any strong interactions with its components.

There had been also a debate that zinc ions in the IMS could function as a trap on the *trans* side of the outer membrane to achieve vectorial import of small Tim proteins because small

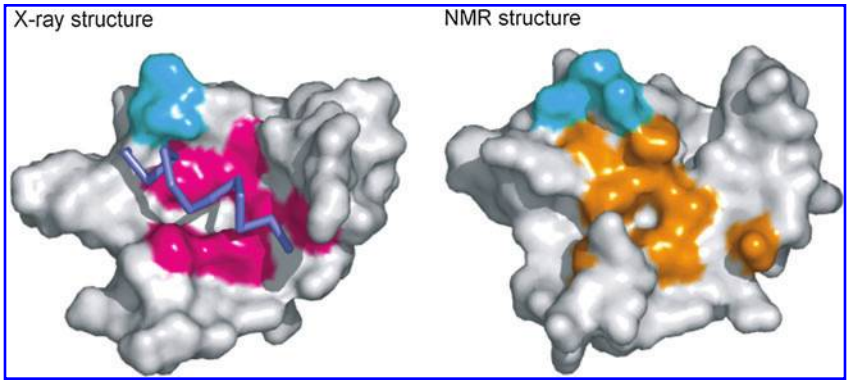

FIG. 8. Putative substrate binding regions of Tim40/Mia40. Molecular surface of the X-ray crystal structure of yeast Tim40/Mia40C4 with the linker segment (*in stick form*) are drawn with the side chains of the residues interacting with the linker segment (*magenta*) and of the CPC motif (*cyan*) (*left panel*). Molecular surface of the solution NMR structure of the human MIA40 core domain is shown with the side chains of the residues corresponding to the putative substrate-binding region in yeast Tim40/Mia40C4 (*orange*) and of the CPC motif (*cyan*) (*right panel*). (For interpretation of the references to color in this figure legend, the reader is referred to the web version of this article at www.liebertonline.com/ars).

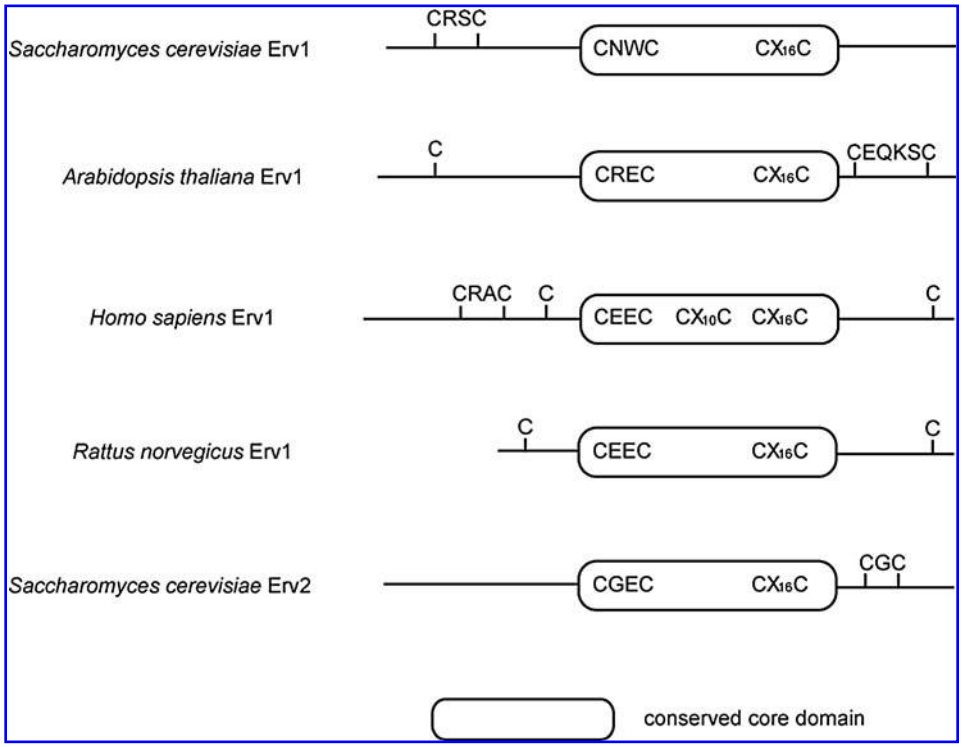

FIG. 9. Schematic diagrams of Erv1/ALR and Erv1-like proteins from various organisms. Conserved FAD-containing core domains are shown as *round boxes* and N-terminal and C-terminal flexible segments as *lines*. Di-cysteine motifs and other cysteine residues are indicated.

Tim proteins can bind zinc ions (46, 55). Although zinc ions can promote efficient import of small Tim proteins *in vitro* (55), small Tim proteins bind to or are chaperoned by zinc ions already in the cytosol, thereby retaining import-competent conformations with reduced cysteinyl thiols (54, 60). This in turn means that in the IMS, excess zinc ions should be removed to facilitate efficient oxidation of cysteinyl thiols in both disulfide donor Tim40/Mia40 and its substrate proteins. Hot13 (*H*elper *o*f *T*im of 13 kDa; 22) was recently suggested to function as a zinc chelator in the IMS (57). Hot13 likely maintains Tim40/Mia40 in a zinc-free state, thereby facilitating its efficient oxidation by Erv1 and subsequent donation of the disulfide linkage to substrate proteins.

Erv1 as Sulfhydryl Oxidase for Tim40/Mia40

While oxidized Mia40 mediates disulfide bond formation in substrate proteins, Erv1 reoxidizes reduced Mia40 for the next round of the Mia40-mediated disulfide transfer (56, 69). Erv1, which is called ALR (*A*ugmenter of *L*iver *R*egeneration) in mammals, is a flavin adenine dinucleotide (FAD)-dependent sulfhydryl oxidase present in the mitochondrial IMS and essential for yeast cell growth (Fig. 9) (13, 52). Erv1 is imported into the IMS and undergoes its own oxidative folding with the aid of Tim40/Mia40 to become functional (74). Erv1 catalyzes the electron transfer from substrate-protein thiols through the noncovalently bound FAD cofactor to molecular oxygen to produce hydrogen peroxide (3, 23) or to oxidized cytochrome *c* (Cyt *c*) to donate electrons to the respiratory chain, which leads to the production of water from molecular oxygen (2, 16, 23, 27). The latter appears more favorable for the electron transfer pathway via Erv1 under physiological conditions. Erv2 in the yeast ER lumen is a paralog of yeast Erv1, although it is not essential for cell viability or respiration (Fig. 9).

High-resolution crystal structures are available for four Erv1 family proteins: *Arabidopsis thaliana* Erv1 (AtErv1) (77), rat ALR (79), yeast Erv1 (Kawano S, Watanabe N, and Endo T, unpublished results), and yeast Erv2 (32). These enzymes form head-to-tail homodimers, each subunit consisting of the core domain of ~100 amino acid residues and flanking flexible segments (Fig. 10) (28). The tightly folded core domain consists of five α-helices, four of which form a bundle that accommodates the isoalloxazine ring of FAD. The core domain contains the 'active-site' disulfide or proximal CXXC motif (Cys130–Cys133 for yeast Erv1), which is juxtaposed with the FAD isoalloxazine ring and is supposed to transfer electrons to flavin. Erv1 and Erv2 contain another disulfide essential for functions *in vivo* (Cys30–Cys33 in yeast Erv1) (32, 36). This disulfide, referred to as the 'shuttle' or 'distal' disulfide, is present in the flexible segment N-terminal (yeast and mammalian Erv1) or C-terminal (plant Erv1 and yeast Erv2) to the core domain (Fig. 9) (51). While being in close proximity to the FAD isoalloxazine ring, the active-site cysteine pair is partly buried and can receive electrons directly from the artificial small substrate DTT, but not from its authentic substrate Tim40/Mia40. Rather, the shuttle disulfide receives electrons from Tim40/Mia40 by forming a transient mixed disulfide intermediate likely involving, for example, Cys30 or Cys33 of yeast Erv1 and C2 of the CPC motif in Tim40/Mia40 (3) (Fig. 11). When both Cys30 and Cys33 of the shuttle disulfide in yeast Erv1 were replaced with serine, the Erv1 mutant was more efficient at DTT oxidation than wild-type Erv1 but was enzymatically inactive toward Tim40/Mia40 oxidation (3). When both Cys130 and Cys133 of the active-site disulfide were replaced with serine, the Erv1 mutant was

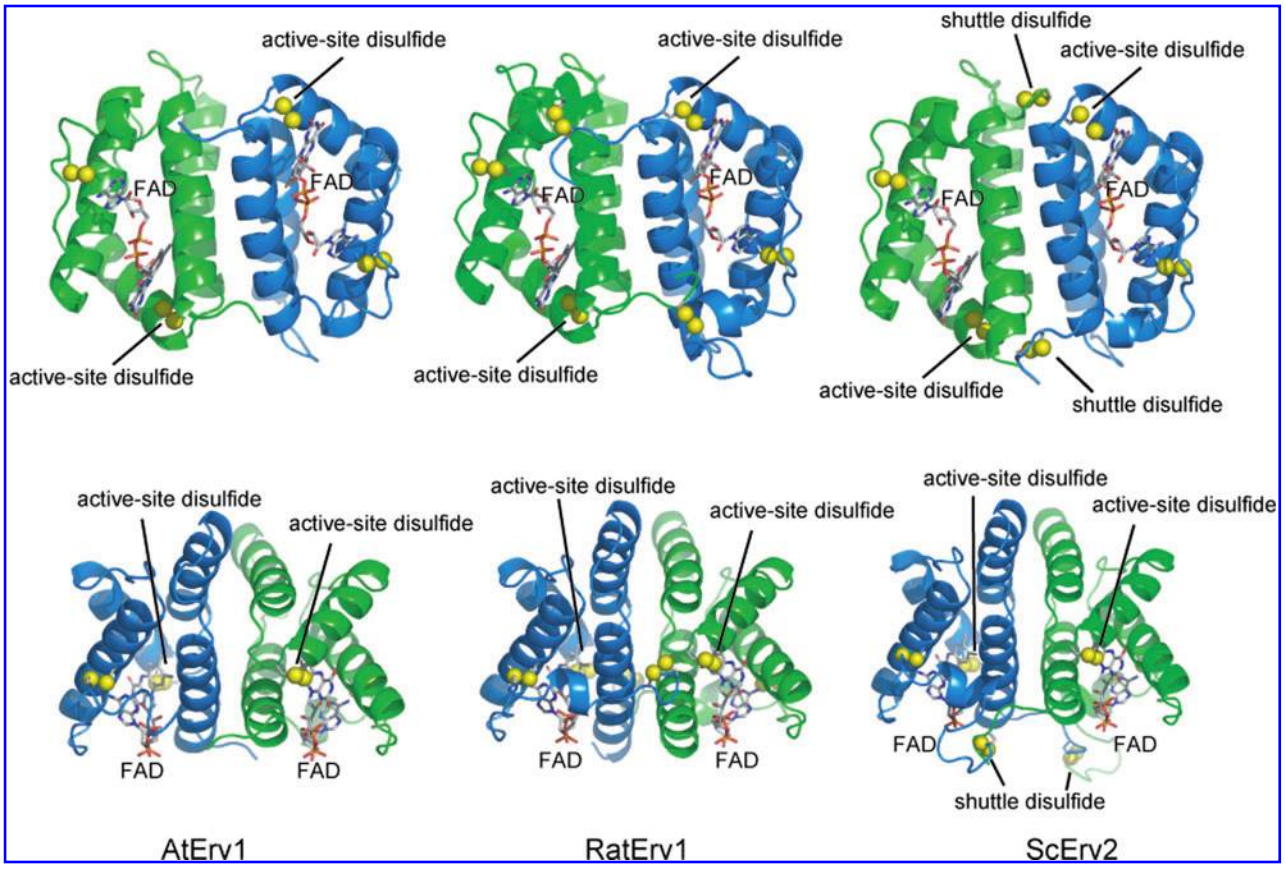

FIG. 10. Comparison of the X-ray crystal structures of Erv1 and Erv1-like proteins. The X-ray crystal structures of *Arabidopsis thaliana* Erv1 (AtErv1; 2HJ3), rat Erv1 (RatErv1; 1OQC), and yeast Erv2 (ScErv2; 1JR8) are shown in *ribbon model* with FAD (*stick form*) and the sulfur atoms of the disulfide bonds (*yellow spheres*). The proteins are viewed (*upper panels*) along their two-fold axes of symmetry (*lower panels*) and along their two-fold axes of symmetry perpendicular to the view in *upper panels*. Two subunits in the homodimer are shown in different colors. (For interpretation of the references to color in this figure legend, the reader is referred to the web version of this article at www.liebertonline.com/ars).

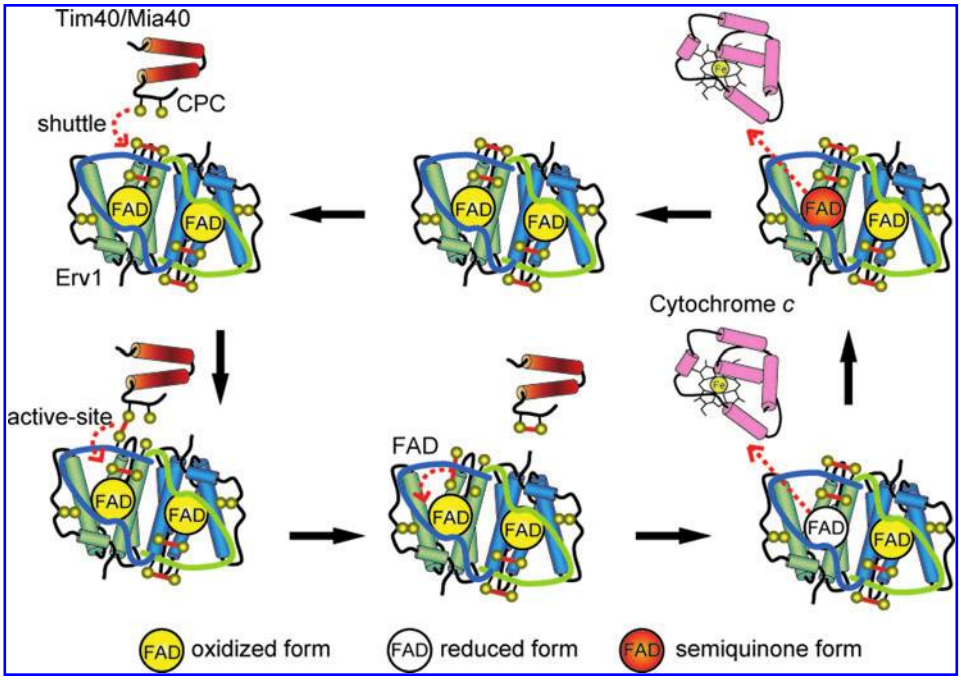

FIG. 11. Electron transfer reactions of Erv1. A current model of electron transfer (the CPC motif of Tim40/Mia40 → the shuttle disulfide of Erv1 → the active-site disulfide in the other subunit of the Erv1 dimer → FAD → the heme of cytochrome *c*) is shown. Note that electron transfer from FAD to cytochrome *c* is two single-electron transfer reactions. α-Helices are shown in cylinders and the S atoms in *yellow spheres*. (For interpretation of the references to color in this figure legend, the reader is referred to the web version of this article at www.liebertonline.com/ars).

quickly reduced *in vitro* upon addition of partially reduced Tim40/Mia40 with reduced C1 and C2, but remained in the reduced form for a longer period and was enzymatically inactive (3). The shuttle disulfide in the one subunit of the Erv1 dimer appears capable of transferring electrons to the active-site disulfide in the other subunit of the homodimer complex (Fig. 11) (24).

After transfer of electrons from Tim40/Mia40 to the oxidized FAD in Erv1 via the shuttle disulfide and active-site disulfide, reduced FAD needs to transfer electrons to an appropriate electron acceptor. Interestingly, yeast Erv2 and AtErv1, both of which can transfer electrons directly to molecular oxygen, possess a short hydrophobic channel leading from the protein surface to the vicinity of the N5 nitrogen of FAD, which may be the route for oxygen to reach the FAD redox center (Fig. 12) (77). On the other hand, rat Erv1, the human ortholog that utilizes oxygen poorly as an electron acceptor, does not have an obvious oxygen channel (Fig. 12) (77). The recently determined X-ray structure of yeast Erv1 also indicates the presence of a possible oxygen channel (Kawano S, Watanabe N, and Endo T, unpublished results), which is consistent with the ability of yeast Erv1 to transfer electrons directly to molecular oxygen (23). Nevertheless, Cyt *c* is a more favorable electron acceptor for Erv1 than molecular oxygen both *in vivo* and *in vitro* (23, 27), which may be important because Cyt *c* as an electron acceptor reduces the potential risk of generation of harmful H_2O_2 (Fig. 11) (23). Although Erv1 can physically interact with Cyt *c* to form a stable 1:1 complex ($K_d \leq 100$ n*M*) (23) the structural details of this Erv1-Cyt *c* interaction remains elusive. It is also to be noted that Cyt *c* reduction is a one-electron reaction while oxidation of the active-site cysteine pair to a disulfide is a two-electron reaction. This is why FAD mediates electron transfer from the active-site disulfide to Cyt *c* because FAD can switch the two-electron reaction to one-electron reaction by transiently forming an FAD semiquinone (24, 27, 79).

Redox Chemistry of the Mitochondrial Disulfide Relay System

Although redox controls in the cytosol and mitochondrial matrix are maintained separately by cytosolic and mitochondrial isoforms of GSSG reductase, the mitochondrial IMS lacks the GSSG reductase activity and is maintained more oxidizing than the cytosol and mitochondrial matrix (39). In the Tim40/Mia40-Erv1 mitochondrial disulfide relay system, disulfide transfer or electron transfer takes place in a linear fashion involving substrate proteins, Tim40/Mia40, and Erv1. The redox potential (E°) for the reduction-sensitive C1–C2 (CPC) disulfide of Tim40/Mia40 (−200 mV) is between those for Tim40/Mia40

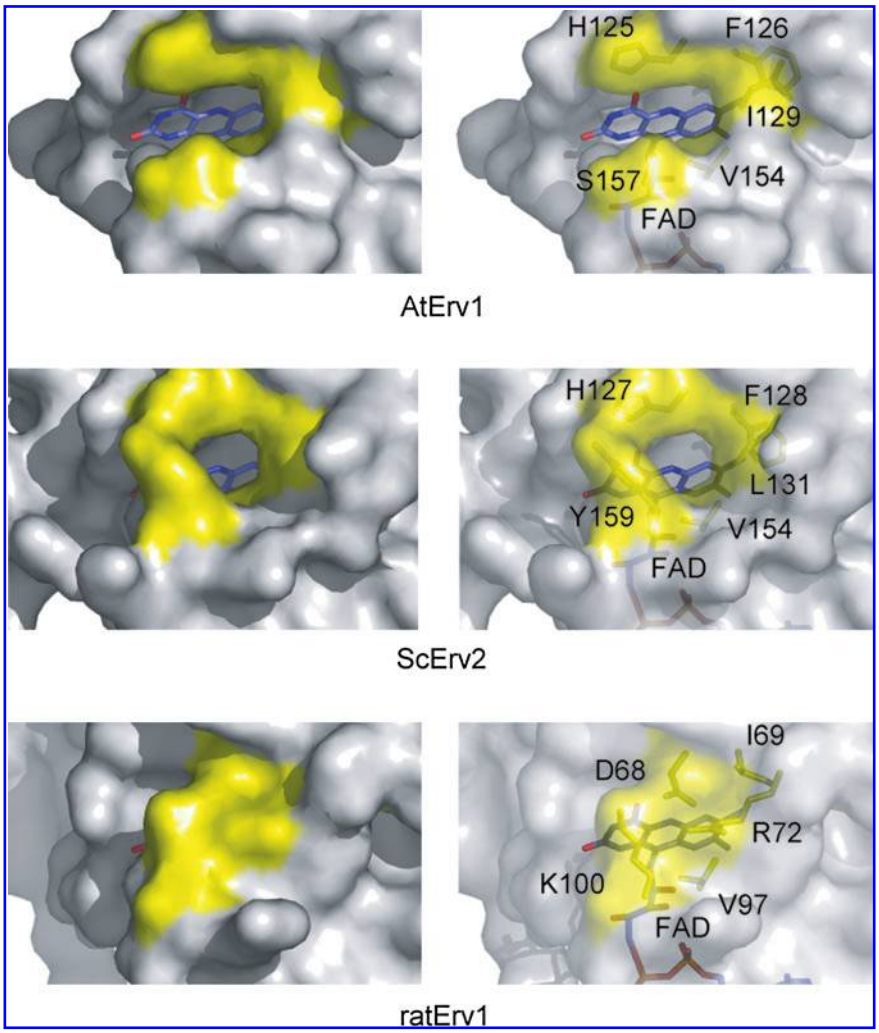

FIG. 12. Putative oxygen channels of Erv1 and Erv2. Putative oxygen channels of AtErv1 and yeast Erv2 (ScErv2) are shown in *yellow* (side chains) with residue numbers (*right panels*) on molecular surfaces and compared with the corresponding region of the rat Erv1 (ratErv1) surface. FAD and side chains of channel-forming residues are shown in *stick form*. Opaque molecular surfaces (*left panels*) and semi-transparent molecular surfaces (*right panels*) are compared. (For interpretation of the references to color in this figure legend, the reader is referred to the web version of this article at www.liebertonline.com/ars).

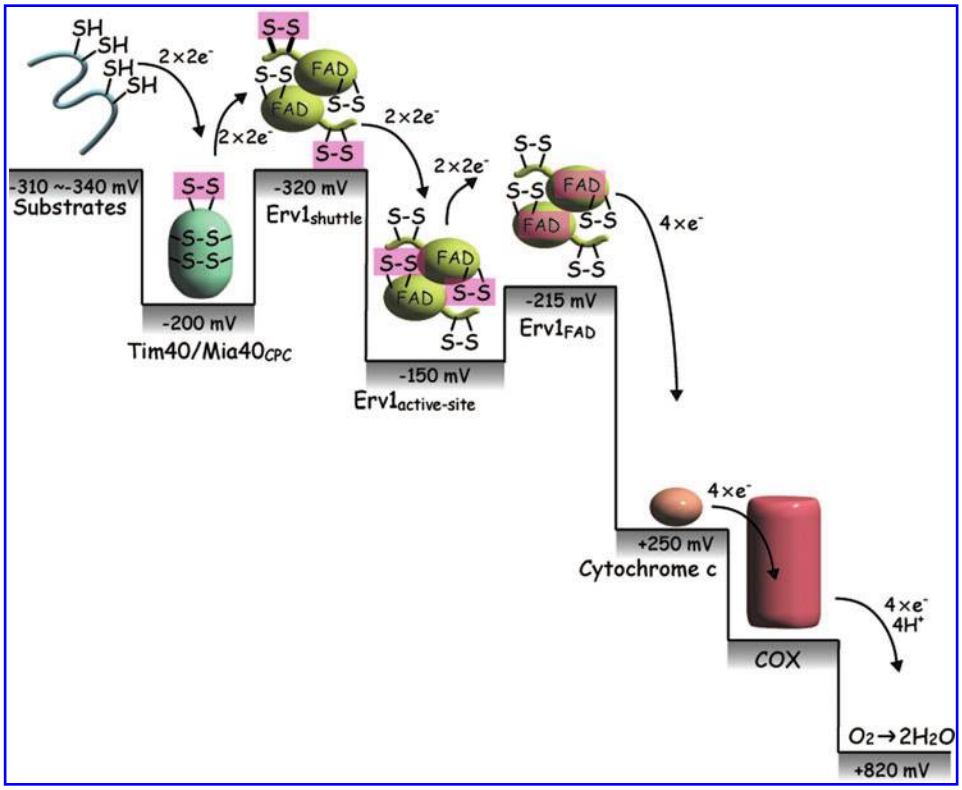

FIG. 13. Schematic of the relative redox potential in the Tim40/Mia40-Erv1 disulfide relay system. See text for details. (For interpretation of the references to color in this figure legend, the reader is referred to the web version of this article at www.liebertonline.com/ars).

substrates (*e.g.*, −340 mV for yeast Cox17, −320 mV for yeast Tim10, and −310 mV for yeast Tim9) and that (−150 mV) for active-site disulfide (C130–C133) in Erv1 (Fig. 13) (10, 23). Those redox potential values thus nicely fit the disulfide relay reactions or direction of electron flow from substrate proteins to Erv1 via Tim40/Mia40 in the mitochondrial IMS.

On the other hand, electron transfer from the C1–C2 disulfide in Tim40/Mia40 ($E^\circ = -200$ mV) to the shuttle disulfide in Erv1 ($E^\circ = -320$ mV) and that from the active-site disulfide ($E^\circ = -150$ mV) to FAD ($E^\circ = -215$ mV) in Erv1 should require mechanisms to overcome the thermodynamically unfavorable redox gradient (Fig. 13) (23). Since redox potentials are experimentally determined by using DTT or glutathione redox buffers, they may well change after possible conformational changes of Erv1 and/or Tim40/Mia40 by, for example, binding of Erv1 to Tim40/Mia40 and by a swing of the flexible segment with the shuttle disulfide toward the active-site disulfide in Erv1. Alternatively, thermodynamically unfavorable electron transfer from the active-site disulfide to FAD may well be driven by coupling with the efficient electron transfer toward the downstream redox centers. Indeed the redox potential values for Cyt *c* and oxygen (+250 mV and +820 mV, respectively) are much higher than that for FAD (−215 mV), which is consistent with the model that both Cyt *c* and oxygen function as efficient electron sink for FAD in Erv1 (Fig. 13) (23).

Many substrate proteins for Tim40/Mia40 have the twin $CX_{3,9}C$ motif, which requires introduction of two disulfide bonds in a coordinated manner (33, 70, 71). Although the first disulfide bond is transferred from Tim40/Mia40 by forming a mixed-disulfide intermediate, the mechanism of the second disulfide bond formation in substrate proteins is unclear. Once the first disulfide bond is formed, the second disulfide-pair cysteines will be brought into positions close enough for facile disulfide bond formation. In the cases of small Tim proteins, the order of disulfide-bond formation is precisely controlled; the internal disulfide bond is formed first, and formation of the disulfide paring of the C-terminal and N-terminal cysteines follows (70). Such second disulfide formation may be further facilitated by oxygen or glutathione, even under reducing environment as in the cytosol (10, 54). Alternatively, Erv1 may be directly involved in formation of the second disulfide although Erv1 alone cannot introduce a disulfide bond into substrate proteins for Tim40/Mia40. Recently, a ternary complex of Erv1, Tim40/Mia40, and a substrate protein was detected *in vitro* during disulfide transfer into the substrate protein when mitochondria with a ruptured outer membrane or with mutant Tim40/Mia40 were used (71). Erv1 was suggested to facilitate formation of the second disulfide bond of the Tim40/Mia40-bound substrate in the ternary complex, which is prerequisite for release of the substrate from Tim40/Mia40 (71).

Outlook

Since Tim40/Mia40, the first component of the disulfide-relay system in the IMS, was identified, increasing knowledge has accumulated on the mechanisms of oxidative folding in mitochondria. However, we are still left with many open questions. Although introduction of covalent disulfide linkages into small IMS proteins clearly contribute to their unidirectional import, it is not clear if this is the only general role of disulfide bonds in IMS proteins. In this connection, it is interesting to note that larger proteins may, like Tim40/Mia40, well require the disulfide-relay system for their formation of internal disulfide bonds, which is nevertheless uncoupled from their import. Indeed, subunits in the cytochrome bc_1 complex

and cytochrome oxidase utilize disulfide bonds for their enzymatic activity and copper acquisition, respectively (46). The IMS as an oxidizing compartment corresponds to the bacterial periplasmic space, which also allows oxidative folding of many proteins, yet the machineries and reactions of the disulfide-relay system in the IMS are quite different from those of the bacterial Dsb system (40). Therefore, how the Tim40/Mia40-Erv1 system in the mitochondrial IMS has developed during evolution of mitochondria from their ancestral prokaryotes is an intriguing question. Whereas the bacterial periplasm and ER lumen contain isomerases that facilitate the reshuffling of disulfide bonds within and between proteins, no isomerase or disulfide reductase has been identified in the mitochondrial IMS. It remains unclear if this means that IMS proteins never fail to form a disulfide linkage between correct pairs of cysteinyl thiols or that GSH diffusing from the cytosol is sufficient to reduce or isomerizes any incorrectly paired cysteins.

Are the ER lumen and mitochondrial IMS the only two eukaryotic compartments that allow oxidation of cysteine thiols? The thylakoid lumen of chloroplasts appears to allow oxidative protein folding as well, yet its oxidation machinery still remains elusive (35). While cysteinyl thiols can be oxidized in some proteins even in the cytosol (65), it is not known if the cytosol has a general machinery for thiol oxidation. Endeavor to address these questions may lead to more surprises in the future.

Acknowledgments

We thank members of the Endo laboratory for discussions and comments. The authors are supported by Grants-in-Aid for Scientific Research from the Ministry of Education, Culture, Sports, Science and Technology of Japan (MEXT).

References

1. Abajian C, Yatsunyk LA, Ramirez BE, and Rosenzweig AC. Yeast Cox17 solution structure and copper (I) binding. *J Biol Chem* 279: 53584–53592, 2004.
2. Allen S, Balabanidou V, Sideris DP, Lisowsky T, and Tokatlidis K. Erv1 mediates the Mia40-dependent protein import pathway and provides a functional link to the respiratory chain by shuttling electrons to cytochrome *c*. *J Mol Biol* 353: 937–944, 2005.
3. Ang SK, and Lu H. Deciphering structural and functional roles of individual disulfide bonds of the mitochondrial sulfhydryl oxidase Erv1p. *J Biol Chem* 284: 28754–28761, 2009.
4. Arnesano F, Balatri E, Banci L, Bertini I, and Winge DR. Folding studies of Cox17 reveal an important interplay of cysteine oxidation and copper binding. *Structure* 13: 713–722, 2005.
5. Baker MJ, Webb CT, Stroud DA, Palmer CS, Frazier AE, Guiard B, Chacinska A, Gulbis JM, and Ryan MT. Structural and functional requirements for activity of the Tim9–Tim10 complex in mitochondrial protein import. *Mol Biol Cell* 20: 769–779, 2009.
6. Balatri E, Banci L, Bertini I, Cantini F, and Ciofi–Baffoni S. Solution structure of Sco1: A thioredoxin-like protein involved in cytochrome *c* oxidase assembly. *Structure* 11: 1431–1443, 2003.
7. Banci L, Bertini I, Cantini F, Ciofi–Baffoni S, Gonnelli L, and Mangani S. Solution structure of Cox11, a novel type of β-immunoglobulin-like fold involved in Cu_B site formation of cytochrome *c* oxidase. *J Biol Chem* 279: 34833–34839, 2004.
8. Banci L, Bertini I, Ciofi–Baffoni S, Gerothanassis IP, Leontari I, Martinelli M, and Wang S. A structural characterization of human SCO2, *Structure* 15: 1132–1140, 2007.
9. Banci L, Bertini I, Ciofi–Baffoni S, Janicka A, Martinelli M, Kozlowski H, and Palumaa P. A structural-dynamical characterization of human Cox17. *J Biol Chem* 283: 7912–7920, 2007.
10. Banci L, Bertini I, Cefaro C, Ciofi–Baffoni S, Gallo A, Martinelli M, Sideris DP, Katrakili N, and Tokatlidis K. MIA40 is an oxidoreductase that catalyzes oxidative protein folding in mitochondria. *Nat Struct Mol Biol* 16: 198–206, 2009.
11. Barros MH, Johnson A, and Tzagoloff A. COX23, a homologue of COX17, is required for cytochrome oxidase assembly. *J Biol Chem* 279: 31943–31947, 2004.
12. Baud C, de Marcos–Lousa C, and Tokatlidis K. Molecular interactions of the mitochondrial Tim12 translocase subunit. *Protein Pept Lett* 14: 597–600, 2007.
13. Becher D, Kricke J, Stein G, and Lisowsky T. A mutant for the yeast scERV1 gene displays a new defect in mitochondrial morphology and distribution. *Yeast* 15: 1171–1181, 1999.
14. Beers J, Glerum DM, and Tzagoloff A. Purification, characterization, and localization of yeast Cox17p, a mitochondrial copper shuttle. *J Biol Chem* 272: 33191–33196, 1997.
15. Beverly KN, Sawaya MR, Schmid E, and Koehler CM. The Tim8–Tim13 complex has multiple substrate binding sites and binds cooperatively to Tim23. *J Mol Biol* 382: 1144–1156, 2008.
16. Bihlmaier K, Mesecke N, Terzyska N, Bien M, Hell K, and Herrmann JM. The disulfide relay system of mitochondria is connected to the respiratory chain. *J Cell Biol* 179: 389–395, 2007.
17. Chacinska A, Pfannschmidt S, Wiedemann N, Kozjak V, Sanjuán–Szklarz LK, Schulze–Specking A, Truscott KN, Guiard B, Meisinger C, and Pfanner N. Essential role of Mia40 in import and assembly of mitochondrial intermembrane space proteins. *EMBO J* 23: 3735–3746, 2004.
18. Chacinska A, Guiard B, Muller JM, Schulze–Specking A, Gabriel K, Kutik S, and Pfanner N. Mitochondrial biogenesis, switching the sorting pathway of the intermembrane space receptor Mia40. *J Biol Chem* 283: 29723–29729, 2008.
19. Chacinska A, Koehler CM, Milenkovic D, Lithgow T, and Pfanner N. Importing mitochondrial proteins: Machineries and mechanisms. *Cell* 138: 628–644, 2009.
20. Curran SP, Leuenberger D, Oppliger W, and Koehler CM. The Tim9p–Tim10p complex binds to the transmembrane domains of the ADP/ATP carrier. *EMBO J* 21: 942–953, 2002.
21. Curran SP, Leuenberger D, Schmidt E, and Koehler CM. The role of the Tim8p–Tim13p complex in a conserved import pathway for mitochondrial polytopic inner membrane proteins. *J Cell Biol* 158: 1017–1027, 2002.
22. Curran SP, Leuenberger D, Leverich EP, Hwang DK, Beverly KN, and Koehler CM. The role of Hot13p and redox chemistry in the mitochondrial TIM22 import pathway. *J Biol Chem* 279: 43744–43751, 2004.
23. Dabir DV, Leverich EP, Kim SK, Tsai FD, Hirasawa M, Knaff DB, and Koehler CM. A role for cytochrome *c* and cytochrome *c* peroxidase in electron shuttling from Erv1. *EMBO J* 26: 4801–4811, 2007.

24. Deponte M and Hell K. Disulfide bond formation in the intermembrane space of mitochondria. *J Biochem* 146: 599–608, 2009.
25. Endo T and Yamano K. Multiple pathways for mitochondrial protein traffic. *Biol Chem* 390: 723–730, 2009.
26. Esaki M, Kanamori T, Nishikawa S, and Endo T. Two distinct mechanisms drive protein translocation across the mitochondrial outer membrane in the late step of the cytochrome b_2 import pathway. *Proc Natl Acad Sci USA* 96: 11770–11775, 1999.
27. Farrell SR and Thorpe C. Augmenter of liver regeneration: A flavin-dependent sulfhydryl oxidase with cytochrome *c* reductase activity. *Biochemistry* 44: 1532–1541, 2005.
28. Fass D. The Erv family of sulfhydryl oxidases. *Biochim Biophys Acta* 1783: 557–566, 2008.
29. Field LS, Furukawa Y, O'Halloran TV, and Culotta VC. Factors controlling the uptake of yeast copper/zinc superoxide dismutase into mitochondria. *J Biol Chem* 278: 28052–28059, 2003.
30. Gabriel K, Milenkovic D, Chacinska A, Müller J, Guiard B, Pfanner N, and Meisinger C. Novel mitochondrial intermembrane space proteins as substrates of the MIA import pathway. *J Mol Biol* 365: 612–620, 2007.
31. Gebert N, Chacinska A, Wagner K, Guiard B, Koehler CM, Rehling P, Pfanner N, and Wiedemann N. Assembly of the three small Tim proteins precedes docking to the mitochondrial carrier translocase. *EMBO Rep* 9: 548–554, 2008.
32. Gross E, Sevier CS, Vala A, Kaiser CA, and Fass F. A new FAD-binding fold and intersubunit disulfide shuttle in the thiol oxidase Erv2p. *Nat Struct Biol* 9: 61–67, 2002.
33. Grumbt B, Stroobant V, Terziyska N, Israel L, and Hell K. Functional characterization of Mia40p, the central component of the disulfide relay system of the mitochondrial intermembrane space. *J Biol Chem* 282: 37461–37470, 2007.
34. Herrmann JM and Köhl R. Catch me if you can! Oxidative protein trapping in the intermembrane space of mitochondria. *J Cell Biol* 176: 559–563, 2007.
35. Herrmann JM, Kauff F, and Neuhaus HE. Thiol oxidation in bacteria, mitochondria and chloroplasts: Common principles but three unrelated machineries. *Biochim Biophys Acta* 1793: 71–77, 2009.
36. Hofhaus G, Lee JE, Tews I, Rosenberg B, and Lisowsky T. The N-terminal cysteine pair of yeast sulfhydryl oxidase Erv1p is essential for *in vivo* activity and interacts with the primary redox centre. *Eur J Biochem* 270: 1528–1535, 2003.
37. Hofmann S, Rothbauer U, Mühlenbein N, Baiker K, Hell K, and Bauer MF. Functional and mutational characterization of human MIA40 acting during import into the mitochondrial intermembrane space. *J Mol Biol* 353: 517–528, 2005.
38. Horn D, Al–Ali H, and Barrientos A. Cmc1p is a conserved mitochondrial twin CX_9C protein involved in cytochrome *c* oxidase biogenesis. *Mol Cell Biol* 28: 4354–4364, 2008.
39. Hu J, Dong L, and Outten CE. The redox environment in the mitochondrial intermembrane space is maintained separately from the cytosol and matrix. *J Biol Chem* 283: 29126–29134, 2008.
40. Inaba K. Disulfide bond formation system in *Escherichia coli*. *J Biochem* 146: 591–597, 2009.
41. Iwata S, Lee JW, Okada K, Lee JK, Iwata M, Rasmussen B, Link TA, Ramaswamy S, and Jap BK. Complete structure of the 11-subunit bovine mitochondrial cytochrome bc_1 complex. *Science* 281: 64–71, 1998.
42. Jan PS, Esser K, Pratje E, and Michaelis G. Som1, a third component of the yeast mitochondrial inner membrane peptidase complex that contains Imp1 and Imp2. *Mol Gen Genet* 263: 483–491 2000.
43. Jin C, Myers AM, and Tzagoloff A. Cloning and characterization of *MRP10*, a yeast gene coding for a mitochondrial ribosomal protein. *Curr Genet* 21: 228–234, 1997.
44. Kawano S, Yamano K, Naoé M, Momose T, Terao K, Nishikawa S, Watanabe N, and Endo T. Structural basis of yeast Tim40/Mia40 as an oxidative translocator in the mitochondrial intermembrane space. *Proc Natl Acad Sci USA* 106: 14403–14407, 2009.
45. Khalimonchuk O, Rigby K, Bestwick M, Pierrel F, Cobine PA, and Winge DR. Pet191 is a cytochrome *c* oxidase assembly factor in *Saccharomyces cerevisiae*. *Eukaryot Cell* 7: 1427–1431, 2008.
46. Koehler CM, Beverly KN, and Leverich EP. Redox pathways of the mitochondrion. *Antioxid Redox Signal* 8: 731–733, 2006.
47. Koehler CM and Tienson HL. Redox regulation of protein folding in the mitochondrial intermembrane space. *Biochim Biophys Acta* 1793:139–145, 2009.
48. LaMarche AE, Abate MI, Chan SH, and Trumpower BL. Isolation and characterization of *COX12*, the nuclear gene for a previously unrecognized subunit of *Saccharomyces cerevisiae* cytochrome *c* oxidase. *J Biol Chem* 267: 22473–22480, 1992.
49. Lamb AL, Wernimont AK, Pufahl RA, Culotta VC, O'Halloran TV, and Rosenzweig AC. Crystal structure of the copper chaperone for superoxide dismutase. *Nat Struct Biol* 6: 724–729, 1999.
50. Lange H, Lisowsky T, Gerber J, Mühlenhoff U, Kispal G, and Lill R. An essential function of the mitochondrial sulfhydryl oxidase Erv1p/ALR in the maturation of cytosolic Fe/S proteins. *EMBO Rep* 2: 715–720, 2001.
51. Levitan A, Danon A, and Lisowsky T. Unique features of plant mitochondrial sulfhydryl oxidase. *J Biol Chem* 279: 20002–20008, 2004.
52. Lisowsky T. Dual function of a new nuclear gene for oxidative phosphorylation and vegetative growth in yeast. *Mol Gen Genet* 232: 58–64, 1992.
53. Longen S, Bien M, Bihlmaier K, Kloeppel C, Kauff F, Hammermeister M, Westermann B, Hermann JM, and Riemer J. Systematic analysis of the twin Cx_9C protein family. *J Mol Biol* 393:356–368, 2009.
54. Lu H and Woodburn J. Zinc binding stabilizes mitochondrial Tim10 in a reduced and import-competent state kinetically. *J Mol Biol* 353: 897–910, 2005.
55. Lutz T, Neupert W, and Herrmann JM. Import of small Tim proteins into the mitochondrial intermembrane space. *EMBO J* 22: 4400–4408, 2003.
56. Mesecke N, Terziyska N, Kozany C, Baumann F, Neupert W, Hell K, and Herrmann JM. A disulfide relay system in the intermembrane space of mitochondria that mediates protein import. *Cell* 121: 1059–1069, 2005.
57. Mesecke N, Bihlmaier K, Grumbt B, Longen S, Terziyska N, Hell K, and Herrmann JM. The zinc-binding protein Hot13 promotes oxidation of the mitochondrial import receptor Mia40. *EMBO Rep* 9:1107–1113, 2008.
58. Milenkovic D, Gabriel K, Guiard B, Schulze–Specking A, Pfanner N, and Chacinska A. Biogenesis of the essential Tim9–Tim10 chaperone complex of mitochondria: site-specific recognition of cysteine residues by the intermembrane space receptor Mia40. *J Biol Chem* 282: 22472–22480, 2007.
59. Milenkovic D, Ramming T, Muller JM, Wenz LS, Gebert N, Schulze–Specking A, Stojanovski D, Rospert S, and Chacinska A. Identification of the signal directing Tim9 and

Tim10 into the intermembrane space of mitochondria. *Mol Biol Cell* 20: 2530–2539, 2009.
60. Morgan B, Ang SK, Yan G, and Lu H. Zinc can play chaperone-like and inhibitor roles during import of mitochondrial small Tim proteins. *J Biol Chem* 284: 6818–6825, 2009.
61. Müller JM, Milenkovic D, Guiard B, Pfanner N, and Chacinska A. Precursor oxidation by Mia40 and Erv1 promotes vectorial transport of proteins into the mitochondrial intermembrane space. *Mol Biol Cell* 19: 226–236, 2008.
62. Naoé M, Ohwa Y, Ishikawa D, Ohshima C, Ishikawa S, Yamamoto H, and Endo T. Identification of Tim40 that mediates protein sorting to the mitochondrial intermembrane space. *J Biol Chem* 279: 47815–47821, 2004.
63. Neupert W and Herrmann JM. Translocation of proteins into mitochondria. *Ann Rev Biochem* 76: 723–749, 2007.
64. Nobrega MP, Bandeira SC, Beers J, and Tzagoloff A. Characterization of *COX19*, a widely distributed gene required for expression of mitochondrial cytochrome oxidase. *J Biol Chem* 277: 40206–40211, 2002.
65. Okazaki S, Tachibana T, Naganuma A, Mano N, and Kuge S. Multiple disulfide bond formation in Yap1 is required for sensing and transduction of H_2O_2 stress signal. *Mol Cell* 27: 675–688, 2007.
66. Reddehase S, Grumbt B, Neupert W, and Hell K. The disulfide relay system of mitochondria is required for the biogenesis of mitochondrial Ccs1 and Sod1. *J Mol Biol* 385: 331–338, 2009.
67. Riemer J, Bulleid N, and Herrmann JM. Disulfide formation in the ER and mitochondria: Two solutions to a common process. *Science* 324: 1284–1287, 2009.
68. Rigby K, Zhang L, Cobine PA, George GN, and Winge DR. Characterization of the cytochrome *c* oxidase assembly factor Cox19 of *Saccharomyces cerevisiae*. *J Biol Chem* 282: 10233–10242, 2007.
69. Rissler M, Wiedemann N, Pfannschmidt S, Gabriel K, Guiard B, Pfanner N, and Chacinska A. The essential mitochondrial protein Erv1 cooperates with Mia40 in biogenesis of intermembrane space proteins. *J Mol Biol* 353: 485–492, 2005.
70. Sideris DP, and Tokatlidis K. Oxidative folding of small Tims is mediated by site-specific docking onto Mia40 in the mitochondrial intermembrane space. *Mol Microbiol* 65: 1360–1373, 2007.
71. Stojanovski D, Milenkovic D, Muller JM, Gabriel K, Schulze–Specking A, Baker MJ, Ryan MT, Guiard B, Pfanner N, and Chacinska A. Mitochondrial protein import: precursor oxidation in a ternary complex with disulfide carrier and sulfhydryl oxidase. *J Cell Biol* 183:195–202, 2008.
72. Stojanovski D, Muller JM, Milenkovic D, Guiard B, Pfanner N, and Chacinska A. The MIA system for protein import into the mitochondrial intermembrane space. *Biochim Biophys Acta* 1783: 610–617, 2008.
73. Terziyska N, Lutz T, Kozany C, Mokranjac D, Mesecke N, Neupert W, Herrmann JM, and Hell K. Mia40, a novel factor for protein import into the intermembrane space of mitochondria is able to bind metal ions. *FEBS Lett* 579: 179–184, 2005.
74. Terziyska N, Grumbt B, Bien M, Neupert W, Hermann JM and Hell K. The sulfhydryl oxidase Erv1 is a substrate of the Mia40-dependent protein translocation pathway. *FEBS Lett* 581: 1098–1102, 2007.
75. Terziyska N, Grumbt B, Kozany C, and Hell K. Structural and functional roles of the conserved cysteine residues of the redox-regulated import receptor Mia40 in the intermembrane space of mitochondria. *J Biol Chem* 284: 1353–1363, 2009.
76. Tsukihara T, Aoyama H, Yamashita E, Tomizaki T, Yamaguchi H, Shinzawa–Itoh K, Nakashima R, Yaono R, and Yoshikawa S. Structures of metal sites of oxidized bovine heart cytochrome *c* oxidase at 2.8 A. *Science* 269: 1069–1074 1995.
77. Vitu E, Bentzur M, Lisowsky T, Kaiser CA, and Fass D. Gain of function in an ERV/ALR sulfhydryl oxidase by molecular engineering of the shuttle disulfide. *J Mol Biol* 362: 89–101, 2006.
78. Webb CT, Gorman MA, Lazarou M, Ryan MT, and Gulbis JM. Crystal structure of the mitochondrial chaperone TIM9•10 reveals a six-bladed α-propeller. *Mol Cell* 21: 123–133, 2006.
79. Wu CK, Dailey TA, Dailey HA, Wang BC, and Rose JP. The crystal structure of augmenter of liver regeneration: A mammalian FAD-dependent sulfhydryl oxidase. *Protein Sci* 12: 1109–1118, 2003.
80. Yamano K, Yatsukawa Y, Esaki M, Hobbs AE, Jensen RE, and Endo T. Tom20 and Tom22 share the common signal recognition pathway in mitochondrial protein import. *J Biol Chem* 283: 3799–3807, 2008.

Address correspondence to:
Toshiya Endo
Department of Chemistry
Graduate School of Science
Nagoya University
Chikusa-ku
Nagoya 464-8602
Japan

E-mail: endo@biochem.chem.nagoya-u.ac.jp

Date of first submission to ARS Central, January 14, 2010; date of acceptance, February 6, 2010.

Abbreviations Used

ALR = augmenter of liver regeneration
Cyt *c* = cytochrome *c*
DTT = dithiothreitol
FAD = flavin adenine dinucleotide
Hot = helper of Tim
IMS = intermembrane space
Mia = mitochondrial intermembrane space import and assembly
Tim = translocase of inner mitochondrial membrane
TM = transmembrane

This article has been cited by:

1. Saikh Jaharul Haque , Tanmay Majumdar , Sailen Barik . 2012. Redox-Assisted Protein Folding Systems in Eukaryotic Parasites. *Antioxidants & Redox Signaling* **17**:4, 674-683. [Abstract] [Full Text HTML] [Full Text PDF] [Full Text PDF with Links]
2. Diana Stojanovski, Piotr Bragoszewski, Agnieszka Chacinska. 2012. The MIA pathway: A tight bond between protein transport and oxidative folding in mitochondria. *Biochimica et Biophysica Acta (BBA) - Molecular Cell Research* **1823**:7, 1142-1150. [CrossRef]
3. Kazutaka Araki , Kenji Inaba . 2012. Structure, Mechanism, and Evolution of Ero1 Family Enzymes. *Antioxidants & Redox Signaling* **16**:8, 790-799. [Abstract] [Full Text HTML] [Full Text PDF] [Full Text PDF with Links] [Supplemental material]
4. Martin van der Laan, Maria Bohnert, Nils Wiedemann, Nikolaus Pfanner. 2012. Role of MINOS in mitochondrial membrane architecture and biogenesis. *Trends in Cell Biology* **22**:4, 185-192. [CrossRef]
5. Emmanouela Kallergi, Maria Andreadaki, Paraskevi Kritsiligkou, Nitsa Katrakili, Charalambos Pozidis, Kostas Tokatlidis, Lucia Banci, Ivano Bertini, Chiara Cefaro, Simone Ciofi-Baffoni, Karolina Gajda, Riccardo Peruzzini. 2012. Targeting and Maturation of Erv1/ALR in the Mitochondrial Intermembrane Space. *ACS Chemical Biology* 120201095624007. [CrossRef]
6. Xiang Ming Xu , Simon Geir Møller . 2011. Iron–Sulfur Clusters: Biogenesis, Molecular Mechanisms, and Their Functional Significance. *Antioxidants & Redox Signaling* **15**:1, 271-307. [Abstract] [Full Text HTML] [Full Text PDF] [Full Text PDF with Links]
7. Matthieu Depuydt , Joris Messens , Jean-Francois Collet . 2011. How Proteins Form Disulfide Bonds. *Antioxidants & Redox Signaling* **15**:1, 49-66. [Abstract] [Full Text HTML] [Full Text PDF] [Full Text PDF with Links]
8. Stephen R. Shouldice , Begoña Heras , Patricia M. Walden , Makrina Totsika , Mark A. Schembri , Jennifer L. Martin . 2011. Structure and Function of DsbA, a Key Bacterial Oxidative Folding Catalyst. *Antioxidants & Redox Signaling* **14**:9, 1729-1760. [Abstract] [Full Text HTML] [Full Text PDF] [Full Text PDF with Links]
9. Toshiya Endo, Koji Yamano, Shin Kawano. 2011. Structural insight into the mitochondrial protein import system. *Biochimica et Biophysica Acta (BBA) - Biomembranes* **1808**:3, 955-970. [CrossRef]
10. Johannes M. Herrmann , Jan Riemer . 2010. The Intermembrane Space of Mitochondria. *Antioxidants & Redox Signaling* **13**:9, 1341-1358. [Abstract] [Full Text HTML] [Full Text PDF] [Full Text PDF with Links]
11. Johannes M. Herrmann , Jan Riemer . 2010. Oxidation and Reduction of Cysteines in the Intermembrane Space of Mitochondria: Multiple Facets of Redox Control. *Antioxidants & Redox Signaling* **13**:9, 1323-1326. [Abstract] [Full Text HTML] [Full Text PDF] [Full Text PDF with Links]